CMS Physics Analysis Summary

Contact: cms-pag-conveners-top@cern.ch 2018/07/04

Measurement of the single top quark and antiquark production cross sections in the t channel and their ratio in pp collisions at $\sqrt{s} = 13\,\text{TeV}$

The CMS Collaboration

Abstract

The cross sections for the production of single top quarks and antiquarks in the t channel, and their ratio, are measured in proton-proton collisions at a center-of-mass energy of 13 TeV. The full data set recorded in 2016 by the CMS detector at the LHC is analyzed, corresponding to an integrated luminosity of 35.9 fb^{-1}. Events with one muon or electron and two jets are selected, where one of the two jets is identified as originating from a bottom quark. A multivariate discriminator exploiting several kinematic variables is applied to separate signal from background events. The ratio $R_{t\text{-ch.}}$ of the cross sections is measured to be $1.65 \pm 0.02\,(\text{stat}) \pm 0.04\,(\text{syst})$. The total cross section for the production of single top quarks or antiquarks is measured to be $219.0 \pm 1.5\,(\text{stat}) \pm 33.0\,(\text{syst})\,\text{pb}$ and the absolute value of the CKM matrix element V_{tb} is determined to be $1.00 \pm 0.05\,(\text{exp}) \pm 0.02\,(\text{theo})$. All results are in agreement with the standard model predictions.

1 Introduction

Top quarks are produced copiously in proton-proton (pp) collisions at 13 TeV center-of-mass energy at the CERN LHC. Studying the production of single top quarks provides crucial insight into the electroweak processes of the standard model of elementary particles (SM) and into the inner structure of the proton. It can also be used for a direct measurement of the Cabibbo–Kobayashi–Maskawa (CKM) matrix element V_{tb}. Out of the three possible production channels, the t-channel process is the dominant mechanism at the LHC and amounts to approximately 70% of the total single top quark production cross section [1]. This channel offers a very distinct signature of a light quark recoiling against the top quark. Figure 1 illustrates the production of a single top quark and the production of a single top antiquark. The flavor of the initial light quark defines the charge of the produced top quark; up-type quarks in the initial state result in a top quark, while down-type quarks produce top antiquarks. The ratio of the cross sections of these two processes, $R_{t\text{-ch.}}$, provides therefore insight into the inner structure of the proton, described by the parton distribution functions (PDFs). The ATLAS and CMS Collaborations have performed several measurements of the cross section for single top quark production in the t channel using LHC data collected at $\sqrt{s} = 7$, 8, and 13 TeV [2–9]. With a data set corresponding to an integrated luminosity of 35.9 fb^{-1}, the analysis described in this article uses roughly 18 times more data compared to the previous analysis at the same center-of-mass energy [9] and makes in addition use of the electron final state. As a result of the increased data set, and because of the cancellation of correlated systematic uncertainties when calculating the ratio of cross sections, the analysis described in this article represents the most precise measurement of $R_{t\text{-ch.}}$ to date.

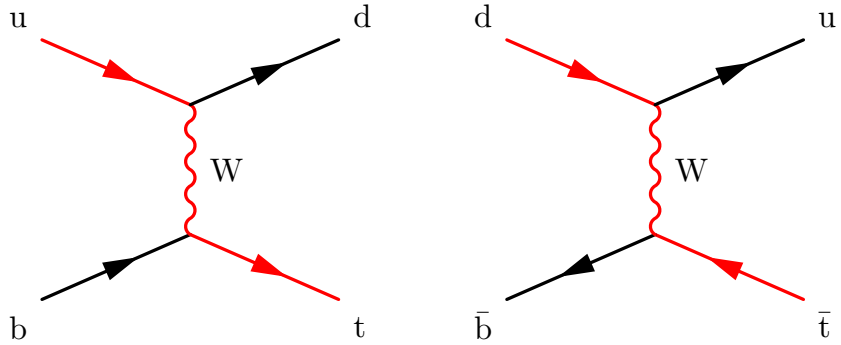

Figure 1: Leading-order Feynman diagrams for the electroweak production of a single top quark (left) and a single top antiquark (right). The flavor of the light quark in the initial state – either up-type (u) or down-type (d) – defines whether a top quark or top antiquark is produced.

The theoretical calculation of the t-channel single top quark process at 13 TeV at next-to-leading-order (NLO) accuracy with HATHOR 2.1 [10, 11] results in cross section values of

$$\begin{aligned}
\sigma_{t\text{-ch.,t}} &= 136.0^{+4.1}_{-2.9}(\text{scale}) \pm 3.5(\text{PDF}+\alpha_s)\ \text{pb}, \\
\sigma_{t\text{-ch.,}\bar{t}} &= \ 81.0^{+2.5}_{-1.7}(\text{scale}) \pm 3.2(\text{PDF}+\alpha_s)\ \text{pb}, \\
\sigma_{t\text{-ch.,t}+\bar{t}} &= 217.0^{+6.6}_{-4.6}(\text{scale}) \pm 6.2(\text{PDF}+\alpha_s)\ \text{pb}
\end{aligned}$$

for the t-channel production of single top quarks, single top antiquarks, and the sum of both subprocesses, respectively. These cross sections are evaluated at a top quark mass of 172.5 GeV, and are performed in the so-called five-flavor scheme (5FS), where the b quark is contained in the PDF of the incoming protons. The uncertainties are associated with the renormalization and factorization scales as well as the strong coupling α_s and the PDF. The latter uncertainties are calculated with the MSTW2008 68% confidence level NLO [12, 13], CT10 NLO [14], and

NNPDF2.3 [15] PDF sets, using the PDF4LHC prescription [16]. Depending on the PDF set used in the calculation, the predicted values for the cross sections of the two processes, and thus also the prediction for their ratio, differ, and the measurement can be used for probing various PDF models. Using the PDF set NNPDF3.0 [17], the predicted value is $R_{t\text{-ch.}} = 1.661 \pm 0.026$.

In the analysis described in this paper, events with a muon or electron in the final state are selected. The muon or electron originates from the decay of the W boson from the top quark decay, either directly or through $W \to \tau\nu$ and following $\tau \to \ell\nu$ decays, where ℓ refers to either a muon or an electron. No attempts are made to distinguish these two cases. The main contributions from background processes that can mimic the signal topology of the analysis come from the production of top quark-antiquark pairs ($t\bar{t}$) and from the production of W bosons in association with jets (W+jets). The separation between signal and background processes is achieved using boosted decision trees (BDTs), which combine the discriminating power of several kinematic distributions into a single classifier. The cross sections of t-channel single top quark and single top antiquark production, as well as the ratio of the two processes, are determined from a fit to the distributions of this single variable.

A description of the CMS detector, together with a definition of the coordinate system used and the relevant kinematic variables, can be found in Ref. [18].

2 Simulation of events

Signal t-channel events are simulated at NLO accuracy with the POWHEG 2.0 [19–22] Monte Carlo (MC) event generator. A comparison with data has shown that p_T and η distributions of the top quark in simulated t-channel events are better modeled in the four-flavor scheme (4FS), where b quarks are not contained in the proton PDFs but produced in gluon splittings, than in the 5FS [23]. Therefore, the 4FS is used for the simulation of t-channel events, while the cross sections calculated in the 5FS are used for the normalization of this sample. The $t\bar{t}$ background process is simulated using POWHEG 2.0 [24], while POWHEG 1.0 [25] is used to generate single top quarks associated to W bosons (tW) in the 5FS. The value of the top quark mass used in the simulated samples is $m_t = 172.5$ GeV. Events with W and Z bosons in association with jets are generated using MG5_AMC@NLO 2.2.2 [26] and the FxFx merging scheme [27]. For all samples, PYTHIA 8.2 [28] is used to simulate parton shower and hadronization. The underlying event is modeled for all samples using the tune CUETP8M1 [29], except for the $t\bar{t}$ sample, for which the tune CUETP8M2T4 [30] is used, providing a more accurate description of the kinematic distributions of the top quark and of the jets in $t\bar{t}$ events. Background events from quantum chromodynamics (QCD) multijet production are modeled using sideband regions in data. The default parameterization of the PDF used in all simulations is NNPDF3.0. All generated events undergo a full simulation of the detector response according to the implementation of the CMS detector within GEANT4 [31]. Additional pp interactions within the same or nearby bunch crossing (pileup) are included in the simulation with the same distribution as observed in data.

3 Event selection and reconstruction

The signature of the single top quark t-channel production process consists of a charged lepton, a corresponding neutrino, which is associated with a transverse momentum imbalance, a light-quark jet, which is often produced in forward direction, and a jet arising from the hadronization of a bottom quark (b jet) from the top quark decay. A second b jet, arising in the production process, generally has a softer p_T spectrum and a broader η distribution compared to the b jet originating from the top quark decay, and therefore often escapes detection. The event selection

criteria are chosen according to this signature and events need to contain one muon or electron candidate and at least two jets. Events in the muon channel are selected using a trigger that requires an isolated muon with $p_T > 24$ GeV. In the electron channel, we use a trigger that requires electrons with $p_T > 32$ GeV and $|\eta| < 2.1$.
Only events for which at least one primary vertex could be reconstructed are considered in the analysis. The primary vertex must be reconstructed from at least four tracks that have a longitudinal distance $|d_z| < 24$ cm and a radial distance $|d_{xy}| < 2$ cm from the interaction point. If more than one primary vertex is found in an event, the reconstructed vertex with the largest value of summed physics-object p_T^2 is taken to be the primary pp interaction vertex.

The particle-flow (PF) algorithm [32], which optimally combines information from all subdetectors, is used for the reconstruction of the individual particles. Muon candidates must have at least one hit in the muon chamber and at least five hits in the silicon tracker. They are then reconstructed by a global fit to the information from the silicon tracker and the muon spectrometer. Selected muons must fulfill the criteria $p_T > 26$ GeV, $|\eta| < 2.4$, and $I_{rel} < 0.06$. The relative isolation I_{rel} of a charged lepton candidate is calculated by summing the transverse energy deposited by charged hadrons, photons, and neutral hadrons around the direction of the lepton, corrected for contributions from pileup, relative to its transverse momentum. Electron candidates are reconstructed by fitting tracks in the silicon tracker using the Gaussian-sum filter [33] and matching the tracks to energy clusters in the ECAL. The electron identification is performed using nine different variables and various selection criteria, including a requirement on the relative isolation of $I_{rel} < 0.06$, as for the muon. Electrons are required to have $p_T > 35$ GeV and $|\eta| < 2.1$, while electrons falling in the gap between the ECAL barrel and endcap regions ($1.44 < |\eta_{SC}| < 1.57$, where SC refers to the ECAL super cluster) are rejected.
Events containing additional muons with $p_T > 10$ GeV and $|\eta| < 2.4$ or additional electrons with $p_T > 15$ GeV and $|\eta| < 2.5$ are rejected. In both cases, the criteria on the lepton identification and isolation are relaxed ($I_{rel} < 0.2$ for muons; $I_{rel} < 0.18$ (0.16) for electrons in the ECAL barrel (endcaps)). Scale factors are applied to correct for inefficiencies in the lepton reconstruction and differences between data and simulation. Jets are clustered using the anti-k_T clustering algorithm [34] with a distance parameter of 0.4, as implemented in the FASTJET package [35]. Using the charged-hadron subtraction technique [36], the contribution from pileup is accounted for. Jet energy corrections are derived from simulation to bring the measured response of jets to that of particle-level jets on average. In situ measurements of the momentum balance in dijet, photon + jet, Z + jet, and multijet events are used to account for any residual differences in the jet energy scale in data and simulation [37]. Additional selection criteria are applied to each jet to remove jets potentially dominated by anomalous contributions from various subdetector components or reconstruction failures. In this analysis, jets with $p_T > 40$ GeV and $|\eta| < 4.7$ are selected. The combined secondary vertex algorithm (CSVv2) is used to identify b jets [38]. The efficiency to identify jets from b quarks is about 40% at the chosen working point, while the efficiency to misidentify jets from light quarks or gluons as b jets is 0.1%. Corrections to the simulation are applied in order to account for differences in the b tagging efficiency in data and simulation.

To suppress the background from QCD multijet processes in the muon channel, the transverse mass of the W boson is used, requiring

$$m_T^W = \sqrt{\left(p_{T,\mu} + p_T^{miss}\right)^2 - \left(p_{x,\mu} + p_{T,x}^{miss}\right)^2 - \left(p_{y,\mu} + p_{T,y}^{miss}\right)^2} > 50 \text{ GeV}. \quad (1)$$

Here, $p_{T,x}^{miss}$ and $p_{T,y}^{miss}$ are the components along the x and y axes, respectively, of the missing transverse momentum vector $\vec{p}_T^{miss}$, which is defined as the projection onto the plane perpen-

dicular to the beam axis of the negative vector sum of the momenta of all reconstructed PF objects in an event. The corresponding components of the momentum vector of the muon are $p_{x,\mu}$ and $p_{y,\mu}$. The magnitude of $\vec{p}_{\mathrm{T}}^{\,\mathrm{miss}}$ is referred to as $p_{\mathrm{T}}^{\mathrm{miss}}$. The energy scale corrections applied to jets are propagated to $p_{\mathrm{T}}^{\mathrm{miss}}$ [39]. To suppress the background from QCD multijet processes in the electron channel, events need to fulfill $p_{\mathrm{T}}^{\mathrm{miss}} > 30$ GeV.

The selected events are divided into four different categories, depending on the number of selected jets and the number of b-tagged jets (n-jets–m-tags). The category with two selected jets, one of which identified as b jet, i.e., 2-jets–1-tag category, provides the largest contribution of signal events constituting the signal category. Events with three selected jets with one or two of them b-tagged, namely events in the 3-jets–1-tag and 3-jets–2-tags categories, are dominated by $\mathrm{t\bar{t}}$ production. They serve as control categories that are used in the fit to constrain the contribution from this main background process. Besides these three categories, which are used to determine the signal and background contributions, a fourth category containing events with two selected jets and no identified b jets, the 2-jets–0-tags category, is used to validate the estimation of the QCD multijet background contribution in data.
The numbers of selected events in the 2-jets–1-tag category are shown in Table 1 for the muon and electron channels. In both channels, the event yields are shown separately for events with positively and negatively charged muons (electrons). Positively charged leptons stem from top quarks and negatively charged leptons from top antiquarks. The event yield of the QCD multijet background is determined directly from data. For the other processes, the event yields are derived from the simulation.

The momentum four-vector of the top quark is reconstructed from the momenta of its decay products: the charged lepton, the corresponding reconstructed neutrino, and the b jet. The ambiguity of the assignment of one of the two b-tagged jets to the b quark from the top quark decay in the 3-jets–2-tags category is solved by choosing the b jet that leads to a reconstructed top quark mass closer to the top quark mass used in the simulation. The momentum of the neutrino can be obtained from the $\vec{p}_{\mathrm{T}}^{\,\mathrm{miss}}$. Assuming energy-momentum conservation at the W$\ell\nu$ vertex and setting the W boson mass to $m_{\mathrm{W}} = 80.4$ GeV, the longitudinal momentum of the neutrino $p_{z,\nu}$ can be calculated as:

$$p_{z,\nu} = \frac{\Lambda p_{z,\ell}}{p_{\mathrm{T},\ell}^2} \pm \frac{1}{p_{\mathrm{T},\ell}^2}\sqrt{\Lambda^2 p_{z,\ell}^2 - p_{\mathrm{T},\ell}^2(p_\ell^2 p_{\mathrm{T}}^{\mathrm{miss}2} - \Lambda^2)}, \tag{2}$$

where

Table 1: Event yields for the relevant processes in the 2-jets–1-tag category after applying the full event selection in the muon and electron channels for an integrated luminosity of 35.9 fb^{-1}. Statistical and systematic uncertainties are considered. The yields are obtained from simulation (using the 4FS prediction for the t-channel signal process and 5FS for the tW process), except for the QCD multijet contribution, which is derived from data (see Section 4).

Process	μ^+	μ^-	e^+	e^-
Top quark pair production	81172 ± 13480	81572 ± 13517	64839 ± 10331	65205 ± 10185
tW	8755 ± 1799	8762 ± 1843	6837 ± 1406	6885 ± 1387
W/Z+jets	38199 ± 12334	33373 ± 10568	23907 ± 8064	21494 ± 6811
QCD	6732 ± 3241	6713 ± 3235	11282 ± 5430	10605 ± 5109
Single top quark t-channel	23628 ± 2918	14574 ± 1883	15103 ± 1840	9395 ± 1188
Total expected	158486 ± 18870	144994 ± 17658	121969 ± 14374	113584 ± 13400
Observed	166446	151440	124857	116206

$$\Lambda = \frac{m_{\mathrm{W}}^2}{2} + \vec{p}_{\mathrm{T},\ell} \cdot \vec{p}_{\mathrm{T}}^{\,\mathrm{miss}} \,, \tag{3}$$

and $p_\ell^2 = p_{\mathrm{T},\ell}^2 + p_{z,\ell}^2$ denotes the squared momentum of the corresponding charged lepton ℓ. In general, this procedure results in two possible solutions for $p_{z,\nu}$, which can have either real or complex values. If both solutions take real values, the one with the smallest absolute value is chosen [40, 41]. In the case of complex solutions, $\vec{p}_{\mathrm{T}}^{\,\mathrm{miss}}$ is modified such that the determinant in Eq. (2) becomes null, while still fulfilling the constraint on the W boson mass. Of the possible solutions for $p_{x,\nu}$ and $p_{y,\nu}$ that resolve the problem of the negative determinant, the coordinate pair that is closest to the corresponding components of $\vec{p}_{\mathrm{T}}^{\,\mathrm{miss}}$ is chosen.

4 Modeling and estimation of the QCD multijet background

The large cross section and the large rejection power of the final event selection for the QCD multijet processes makes it impossible to generate samples of simulated events in reasonable size. To overcome this difficulty, this background contribution is suppressed as much as possible and the remaining contamination is estimated directly from data. As described in Section 3, requirements on $m_{\mathrm{T}}^{\mathrm{W}}$ ($p_{\mathrm{T}}^{\mathrm{miss}}$) are applied on the events in the muon (electron) channel to suppress events from QCD multijet production. These variables provide the highest separation power between QCD multijet events and other processes including the t-channel single top quark process for the respective lepton final state. The same variables are used to estimate the remaining contribution by fitting their distributions over the entire range, i.e., without applying the described requirements. A maximum likelihood fit is performed on the $m_{\mathrm{T}}^{\mathrm{W}}$ ($p_{\mathrm{T}}^{\mathrm{miss}}$) distribution using two probability distribution functions, one for the QCD multijet process and one for all other processes. The latter distribution is obtained by adding the different non-QCD contributions from simulation, including the t-channel signal, according to their theory predictions, while the former is derived from a sideband region enriched in QCD multijet events. This sideband region is defined by inverting the muon or electron isolation requirements. The fit is performed separately in the 2-jets–1-tag and the 3-jets–1-tag categories. The contribution from QCD multijet events to the 3-jets–2-tags category is only minor and is neglected. To validate the described QCD estimation procedure, this fit is also performed in the 2-jets–0-tags category, which features a significantly larger fraction of this background source than the other categories. Good agreement between the results of the fit and the data is found. Figure 2 shows the fitted $m_{\mathrm{T}}^{\mathrm{W}}$ and $p_{\mathrm{T}}^{\mathrm{miss}}$ distributions in the 2-jets–1-tag, 3-jets–1-tag, and 2-jets–0-tags categories. The entire range of the distributions is fitted and the resulting yields of the QCD multijet contribution are then used in the signal regions in which the requirements $m_{\mathrm{T}}^{\mathrm{W}} > 50\,\mathrm{GeV}$ ($p_{\mathrm{T}}^{\mathrm{miss}} > 30\,\mathrm{GeV}$) are applied. In this extrapolation, an uncertainty of 50% is applied to cover all effects from variations in the shape and rate of this background process.

5 Signal extraction

In this analysis, BDT algorithms, implemented in the TMVA package [42], are used to combine multiple variables into single discriminators and thus enhance the separation between signal and background processes. Kinematic variables that are suitable to distinguish the single top quark t-channel signal process from the main background contributions are chosen for the BDT training. These variables are found to provide a reasonable modeling when comparing the simulated events to data. In Table 2 the kinematic variables used for discrimination are listed. The lepton $|\eta|$ and $m_{\mathrm{T}}^{\mathrm{W}}$ distributions are only considered in events with muons, while

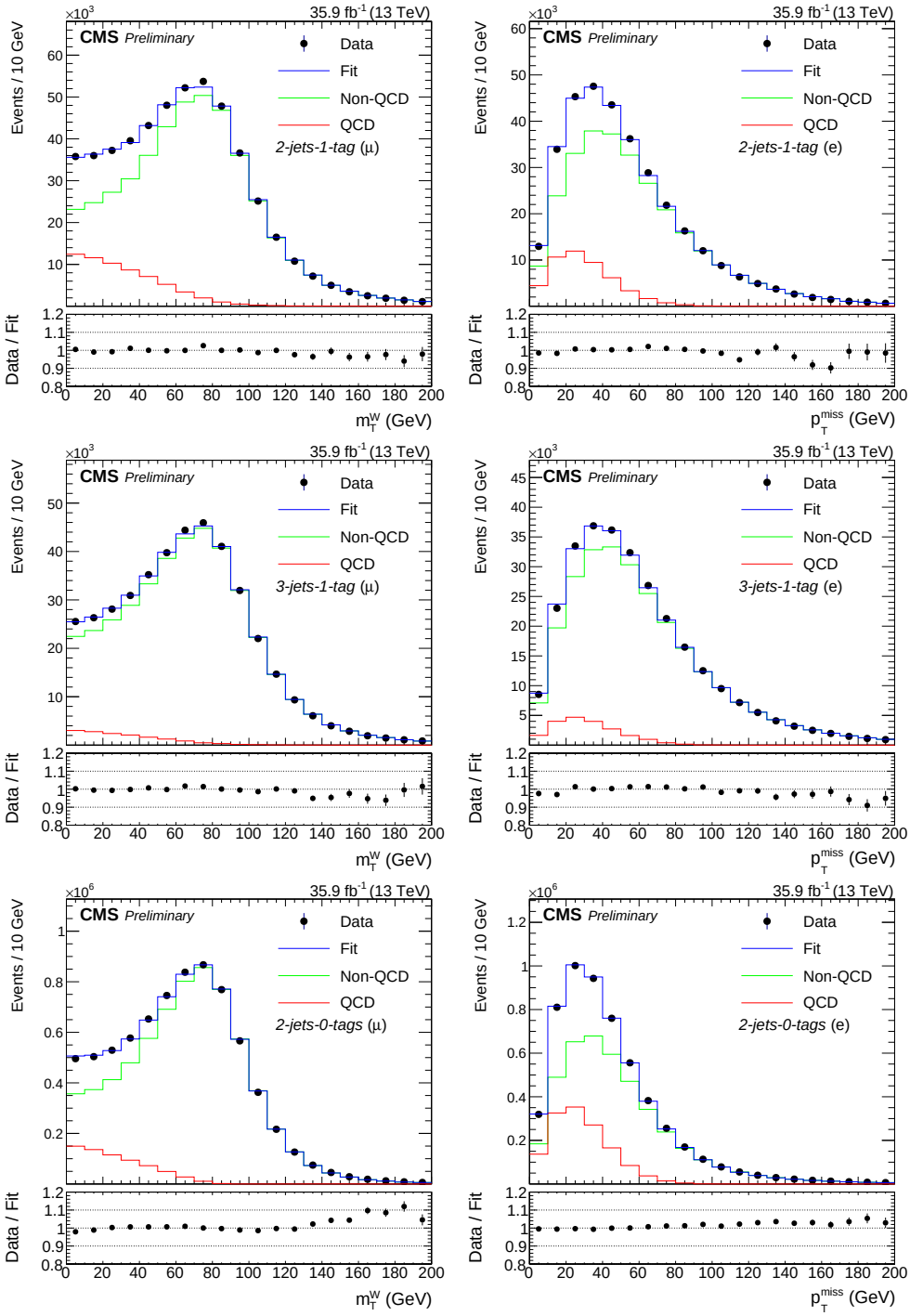

Figure 2: Fit to the $m_{\mathrm{T}}^{\mathrm{W}}$ distribution for events with muons (left) and to the $p_{\mathrm{T}}^{\mathrm{miss}}$ distribution for events with electrons (right) in the 2-jets–1-tag (upper row), 3-jets–1-tag (middle row), and the 2-jets–0-tags categories. The QCD template is extracted from a sideband region in data. For the fit, only statistical uncertainties are considered.

the $p_{\mathrm{T}}^{\mathrm{miss}}$ variable is only used in events with an electron. The five most important variables are the light-quark jet $|\eta|$, as the light-quark jet in the forward direction is a unique feature of the t-channel process, the invariant mass of dijet system consisting of the light-quark jet and the b-tagged jet from the top quark decay, the reconstructed top quark mass, which has high discrimination power against background processes where no top quarks are produced, the distance in the η-ϕ plane ($\Delta R = \sqrt{\Delta\eta^2 + \Delta\phi^2}$) between the charged lepton and the b jet, and the cosine of the angle between the charged lepton and the light-quark jet in the rest frame of the top quark ($\cos(\theta^*)$). Figures 3 and 4 show the distributions of these five input variables from data compared to the simulation.

The BDTs are trained in the 2-jets–1-tag category, separately for muons and electrons. Half of the simulated signal and background events (and in case of the QCD multijet background, half of the data sample from a sideband region in data) are used for the training, while the other half is used for validation purpose and the actual measurement. The BDTs show comparable performance on the training and validation samples and no sign of overtraining is observed. The trained BDTs are then applied to the 2-jets–1-tag, 3-jets–1-tag, and 3-jets–2-tags categories, separately for the two different flavors and charges of the lepton.

A maximum likelihood fit is performed simultaneously on the twelve different BDT output distributions (two lepton charges, two lepton flavors, three n-jets–m-tags categories). By including the categories with three selected jets in the fit, the $\mathrm{t\bar{t}}$ background, which dominates these categories, is constrained. Free parameters of the fit are the scale factors for the cross sections of the t-channel top quark and top antiquark processes and the scale factor for the ratio $R_{t\text{-ch.}}$. The scale factors are defined as the fitted value divided by the predicted value. First, the scale factors for $R_{t\text{-ch.}}$ and for single top antiquark production are fitted simultaneously. In a second fit, the scale factor for $R_{t\text{-ch.}}$ is replaced by the scale factor for the production of single top quarks. This second fit reproduces by construction the result for $R_{t\text{-ch.}}$, yielding in addition a value for the cross section of the production of single top quarks, consistent with the other two results. The benefit of this two-fit procedure is that all correlations of uncertainties between the free parameters are automatically taken into account in a consistent way. The fitted distributions of the BDT outputs are shown in Figs. 5 and 6.

6 Systematic uncertainties

Several sources of systematic uncertainties are considered in the analysis, either as nuisance parameters in the fit of the BDT discriminator distributions (profiled uncertainties) or as external uncertainties. The latter category includes the uncertainty sources related to the modeling of the signal process, which can not be constrained from the measurement as they apply to the full phase space and not only to the region in which the measurement is performed. Their impact is determined by repeating the analysis using varied templates according to the systematic uncertainty sources under study in the fit instead of the nominal templates. The uncertainty due to a certain source is then taken as half the difference between the results for up and down variations of the effect. The uncertainty due to the luminosity is not included in the fit. In the following, the different uncertainty sources that are considered in the analysis are briefly described. For the sake of simplicity and better readability, they are grouped in categories of related sources.

Profiled uncertainties

- **Jet energy scale (JES):** All reconstructed jet four-momenta in simulated events are simultaneously varied according to the p_{T}- and η-dependent uncertainties in the

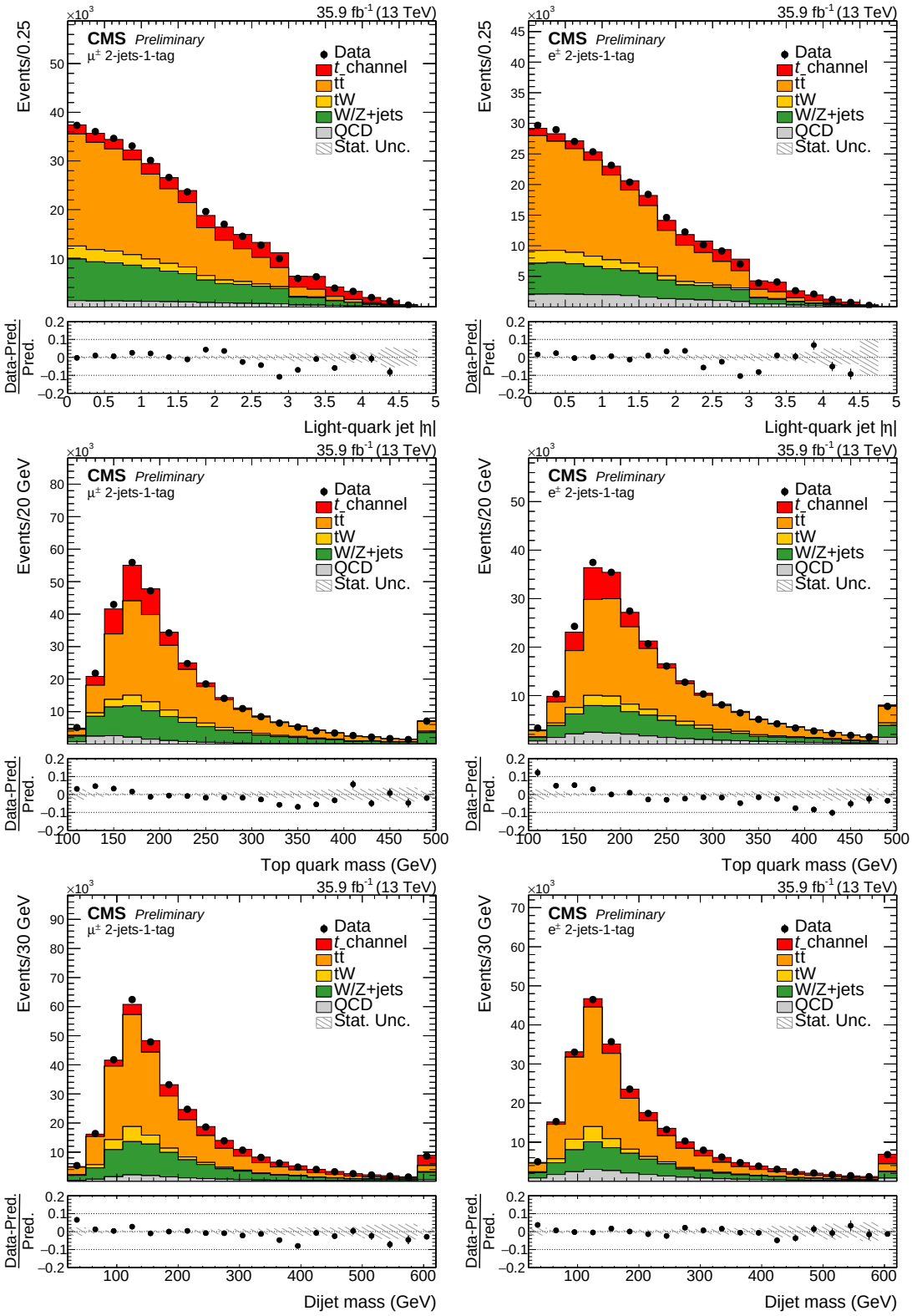

Figure 3: The three most important input variables for the training of the BDTs in the muon channel (left) and in the electron channel (right). The variables are ordered by their importance in the training. The simulation is normalized to the amount of data. The shaded areas correspond to the statistical uncertainties.

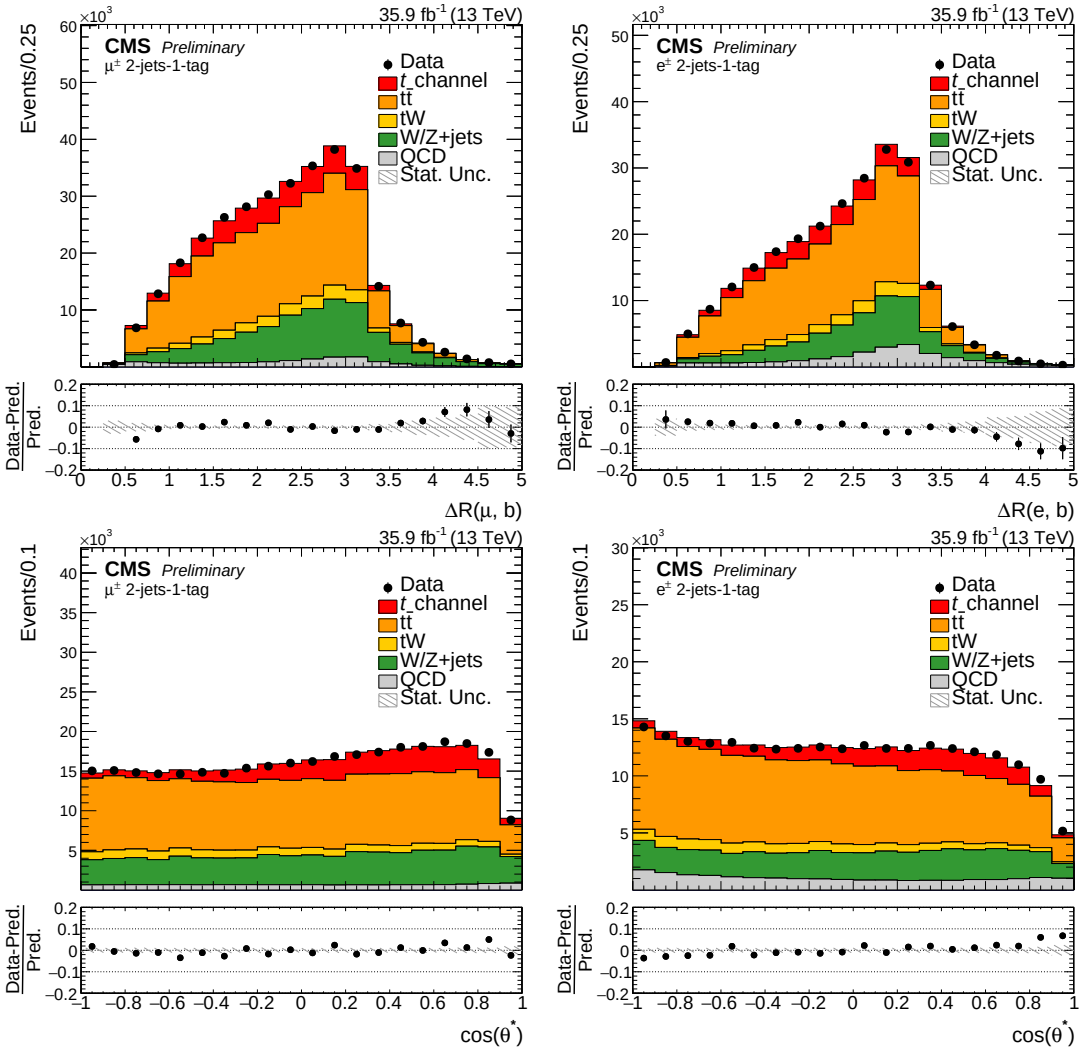

Figure 4: The fourth and fifth most important input variables for the training of the BDTs in the muon channel (left) and in the electron channel (right). The simulation is normalized to the amount of data. The shaded areas correspond to the statistical uncertainties.

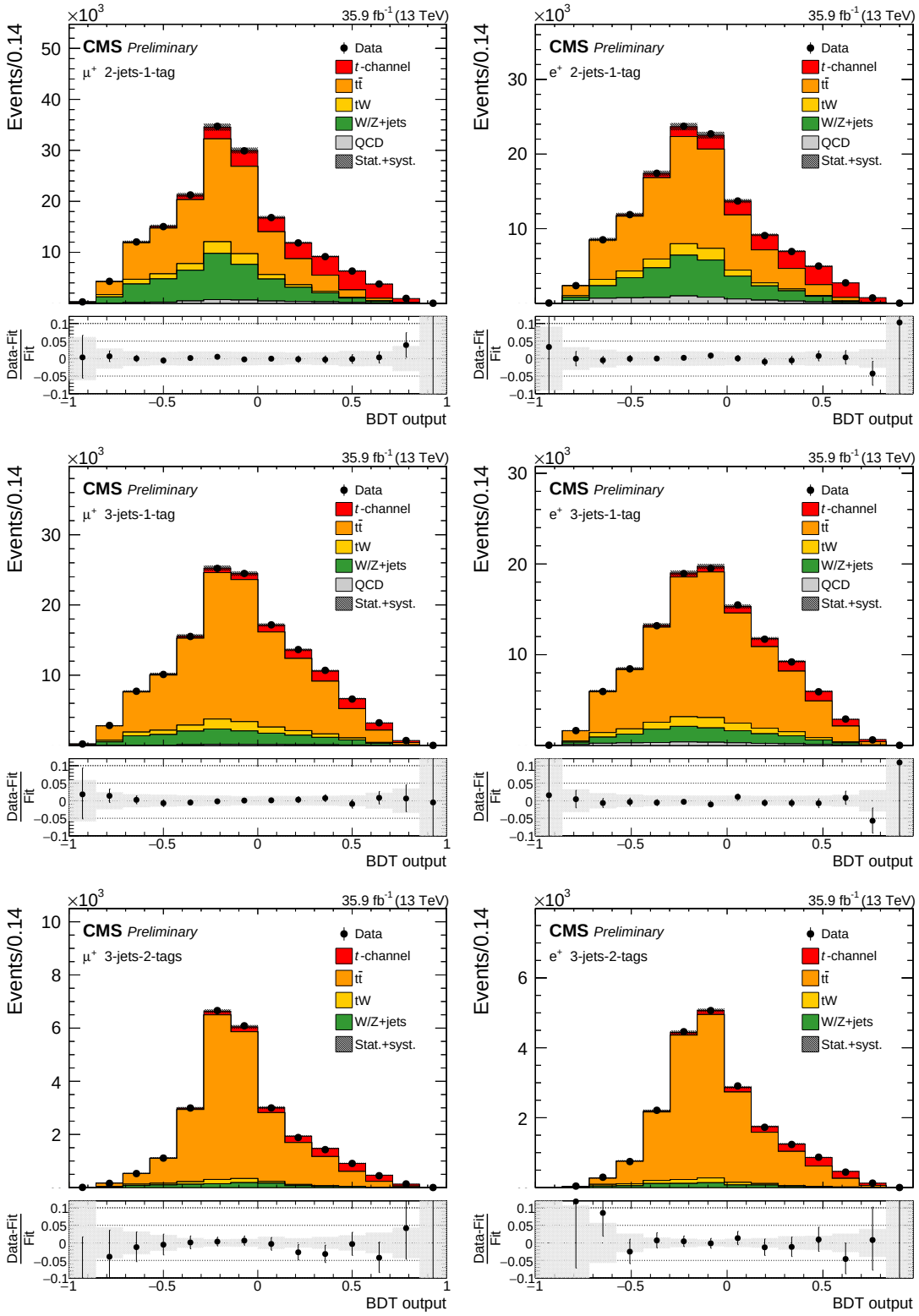

Figure 5: BDT output distribution in the 2-jets–1-tag category (upper row), the 3-jets–1-tag category (middle row), and the 3-jets–2-tags categroy (lower row) for positively charged muons (left column) and electrons (right column). The different processes are scaled to the corresponding fit results. In each figure, the relative difference between the fitted distribution and the distribution in data is shown. The shaded areas correspond to the post-fit uncertainties.

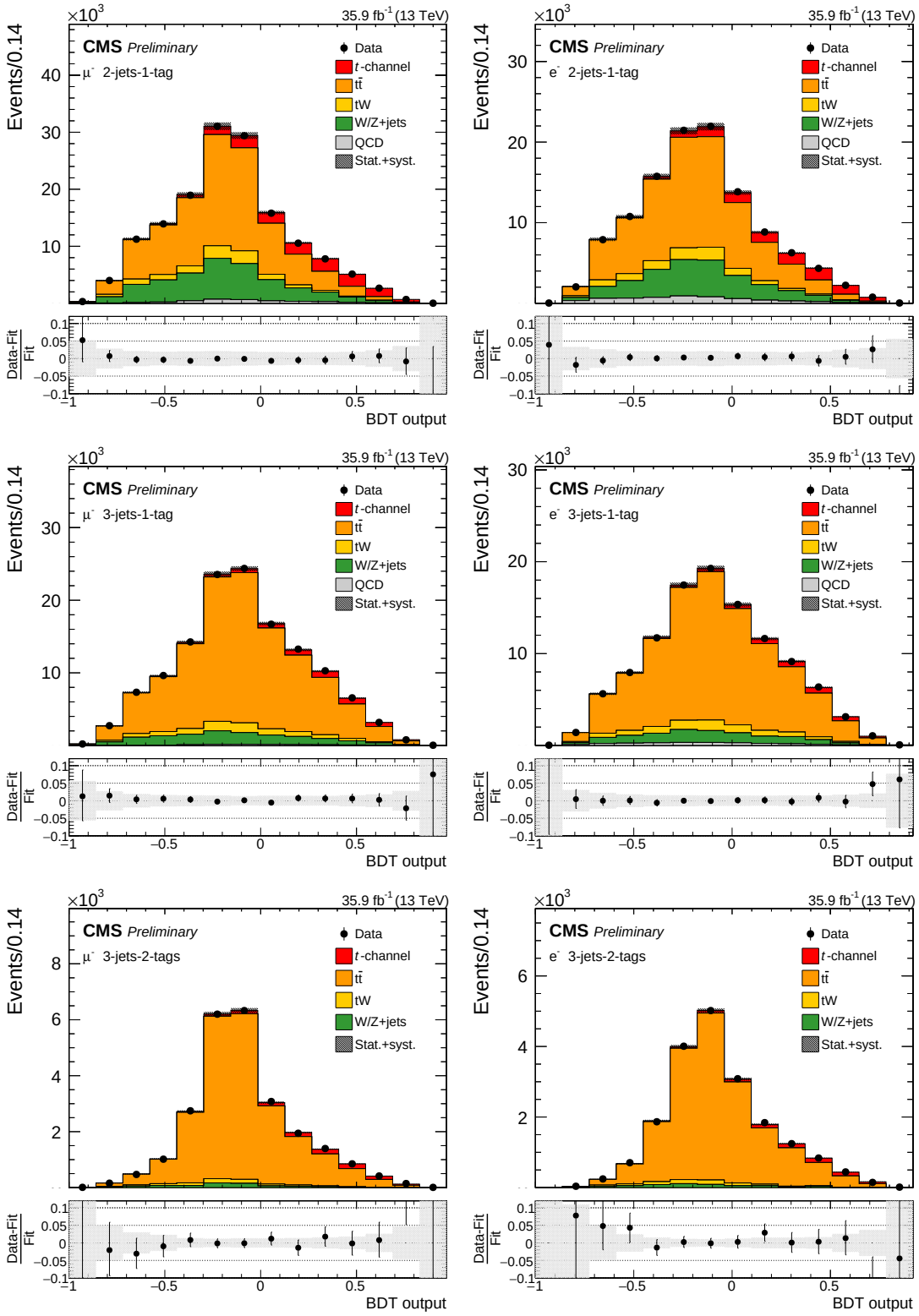

Figure 6: BDT output distribution in the 2-jets–1-tag category (upper row), the 3-jets–1-tag categroy (middle row), and the 3-jets–2-tags category (lower row) for negatively charged muons (left column) and electrons (right column). The different processes are scaled to the corresponding fit results. In each figure, the relative difference between the fitted distribution and the distribution in data is shown. The shaded areas correspond to the post-fit uncertainties.

Table 2: Input variables for the BDTs. The variables $m_{\mathrm{T}}^{\mathrm{W}}$ and lepton $|\eta|$ are only used in the training of events with a muon, while $p_{\mathrm{T}}^{\mathrm{miss}}$ is only used as input for events with an electron.

Variable	Description
Light-quark jet $\|\eta\|$	Absolute value of the pseudorapidity of the light-quark jet
Dijet mass	Invariant mass of the light-quark jet and the b-tagged jet associated to the top quark decay
Top quark mass	Invariant mass of the top quark reconstructed from the lepton, the neutrino and the b-tagged jet associated to the top quark decay
ΔR (lepton, b jet)	ΔR between the momentum vectors of the lepton and the b-tagged jet associated to the top quark decay
$\cos(\theta^*)$	Cosine of the angle between the lepton and the light-quark jet in the rest frame of the top quark
Jet p_{T} sum	Scalar sum of the transverse momentum of the light-quark jet and the b-tagged jet associated to the top quark decay
$m_{\mathrm{T}}^{\mathrm{W}}$	Transverse mass of the W boson
$p_{\mathrm{T}}^{\mathrm{miss}}$	Missing momentum in the transverse plane of the event
ΔR (light jet, b jet)	ΔR between the momentum vectors of the light-quark jet and the b-tagged jet associated to the top quark decay
Lepton $\|\eta\|$	Absolute value of the pseudorapidity of the selected lepton
W boson $\|\eta\|$	Absolute value of the pseudorapidity of the reconstructed W boson
Light-quark jet mass	Invariant mass of the light-quark jet

JES [43]. These variations are also propagated to $p_{\mathrm{T}}^{\mathrm{miss}}$.

- **Jet energy resolution (JER):** To account for the difference in the JER between data and simulation, a dedicated smearing is applied to the simulated jets [43], increasing or decreasing the resolutions within their uncertainties.
- **Unclustered energy:** The contributions of unclustered particles to $p_{\mathrm{T}}^{\mathrm{miss}}$ are varied within their respective energy resolutions [44].
- **Muon and electron efficiencies:** The efficiencies of the lepton identification and isolation, of the used trigger paths, and of the tracker response are determined with a "tag-and-probe" method [45] from Drell–Yan events falling into the Z boson mass window. The efficiency correction factors are varied according to the p_{T}- and η-dependent uncertainties.
- **Pileup:** The uncertainty in the average expected number of pileup interactions is propagated as a systematic uncertainty to this measurement by varying the minimum-bias cross section by $\pm 4.6\%$ [46].
- **b tagging:** The scale factors that are used to calculate the efficiency corrections of the CSVv2 b tagging algorithm are varied up and down within their uncertainties. From these up and down varied scale factors, up- and down-shifted efficiency corrections are calculated and applied to the simulation.
- **QCD normalization:** As described in Section 4, an uncertainty of $\pm 50\%$ is applied on the QCD background estimation to fully cover all effects from variations in the

shape and rate of this process.

- **Limited size of samples of simulated events:** The limited number of available simulated events is considered by performing the fit using the Barlow–Beeston method [47].
- **$\mathrm{t\bar{t}}$ modeling and normalization:** The influence of the parton shower scale and of the matching between the NLO calculation and the parton shower is estimated using systematically shifted $\mathrm{t\bar{t}}$ samples. Furthermore, the impact of variations in the initial-state and final-state radiation, depending on the choice of α_s, and the effect of uncertainties on the modeling of the underlying event are studied by comparing the nominal sample with dedicated $\mathrm{t\bar{t}}$ samples. To account for the uncertainty in the $\mathrm{t\bar{t}}$ cross section, a rate uncertainty of $\pm5\%$, corresponding to the precision of the most precise measurement [48], is applied.
- **Top quark p_T:** In differential measurements of the top quark p_T in $\mathrm{t\bar{t}}$ events, the predicted p_T spectrum is found to be harder than the observed spectrum [49]. To account for this mismodeling, the results derived using the default simulation for $\mathrm{t\bar{t}}$ are compared to the results using simulated $\mathrm{t\bar{t}}$ events that are reweighted according to the observed difference between data and simulation in Refs. [49–51].
- **W/Z + jets normalization:** To take the uncertainty in the cross sections of the W + jets and Z + jets contributions into account, rate uncertainties of $\pm5\%$, corresponding to the most precise measurements [52], are applied.
- **tW normalization:** To account for the uncertainty in the cross section of tW production, a rate uncertainty of $\pm11\%$, corresponding to the precision of the most precise measurement [53], is applied. One additional rate uncertainty is included in the fit to account for the impact from the choice of PDFs and their specific variation ($\pm4\%$). To determine the influence of possible mismodeling of the tW process, the nominal sample is compared to samples generated with a parton shower scale shifted by ±1 standard deviation.
- **Renormalization and factorization scale uncertainty (μ_R/μ_F):** For the background contributions from $\mathrm{t\bar{t}}$, tW, and W/Z + jets production, the uncertainties caused by variations in the renormalization and factorization scales are considered by reweighting the BDT response distributions with different combinations of doubled/halved renormalization and factorization scales [54] with the nominal value set at 172.5 GeV. This uncertainty is estimated for each process separately.
- **Background PDFs:** By reweighting distributions derived from the eigenvector variations of NNPDF 3.0 [16], the impact due to the choice of PDFs is studied for all background processes with the exception of tW production, as the required information is not available in the simulation of this process.

Externalized uncertainties

- **Signal modeling:** The following uncertainty sources cover potential mismodeling of the single top quark *t*-channel signal process. They are not considered as nuisance parameters in the fit but evaluated by repeating the full analysis using samples of simulated signal events that feature variations in the modeling parameters covering the systematic uncertainty sources under study.
    - **Renormalization and factorization scale uncertainty (μ_R/μ_F):** The uncertainties caused by variations in the renormalization and factorization scales are considered by reweighting the BDT response distributions with different combinations of doubled/halved renormalization and factoriza-

tion scales with the nominal value set at 172.5 GeV.

- **Matching of matrix element and parton shower (ME-PS matching):** The parameter that controls the matching between the matrix-element level calculation and the parton shower and regulates the high-p_{T} radiation in the simulation is varied within its uncertainties.
- **Parton shower scale** The renormalization scales of the initial-state and final-state parton shower are varied by facors of two and one half with the nominal value set at 172.5 GeV.

- **Signal PDF:** The impact due to the choice of PDFs is studied by replacing the nominal signal templates with the reweighted distributions derived from the eigenvector variations of NNPDF 3.0 [16].

Uncertainties not included in the fit

- **Luminosity:** The relative uncertainty of the integrated luminosity is determined to be $\pm$2.5% [55]. This uncertainty is added to the total uncertainties of the measured cross sections.

The contributions of the individual sources to the total uncertainty are listed in Table 3 and shown in Fig. 7. The contributions from the profiled uncertainties are estimated by performing the maximum likelihood fit again for each uncertainty source, with the corresponding nuisance parameter fixed to its optimal fit value. The contribution is then calculated as the relative change of the cross sections, or cross section ratio ratio, with respect to the nominal ones. For the externalized uncertainties, the change of the result due to the respective variation is listed. For the sake of simplicity, several nuisance parameters are grouped together in Table 3 and Fig. 7. The dominant uncertainties for the cross section measurements are the uncertainties in the parton shower scale and in the renormalization and factorization scales of the signal modeling, the uncertainty in the jet energy scale, and the uncertainty in the transverse momentum of the top quark in the simulation of the $\mathrm{t\bar{t}}$ background. Because of the cancellation of correlated uncertainties when calculating the ratio of the two cross sections, the signal modeling uncertainties are significantly reduced in the ratio measurement. The only exception to this rule is the uncertainty in the PDF choice which is anticorrelated between the two cross section measurements. Although playing only a minor role in the cross section measurements, this uncertainty source has therefore a relatively high impact on the ratio measurement. The other dominant uncertainties in the ratio measurement are the uncertainty in the normalization of the QCD multijet background, the uncertainty in the jet energy scale, and the uncertainty in the modeling of the $\mathrm{t\bar{t}}$ background.

7 Results

The ratio of the cross section for the production of single top quarks to that for the production of single top antiquarks is measured as

$$\begin{aligned} R_{t\text{-ch.}} &= 1.65 \pm 0.02\,(\text{stat}) \pm 0.03\,(\text{prof}) \pm 0.03\,(\text{ext}) \\ &= 1.65 \pm 0.02\,(\text{stat}) \pm 0.04\,(\text{syst}) \\ &= 1.65 \pm 0.05. \end{aligned}$$

Here, the uncertainty sources that are profiled in the fit, are labeled as “prof”, while the uncertainties on the signal modeling, which are determined externally, are labeled as “ext”. The total

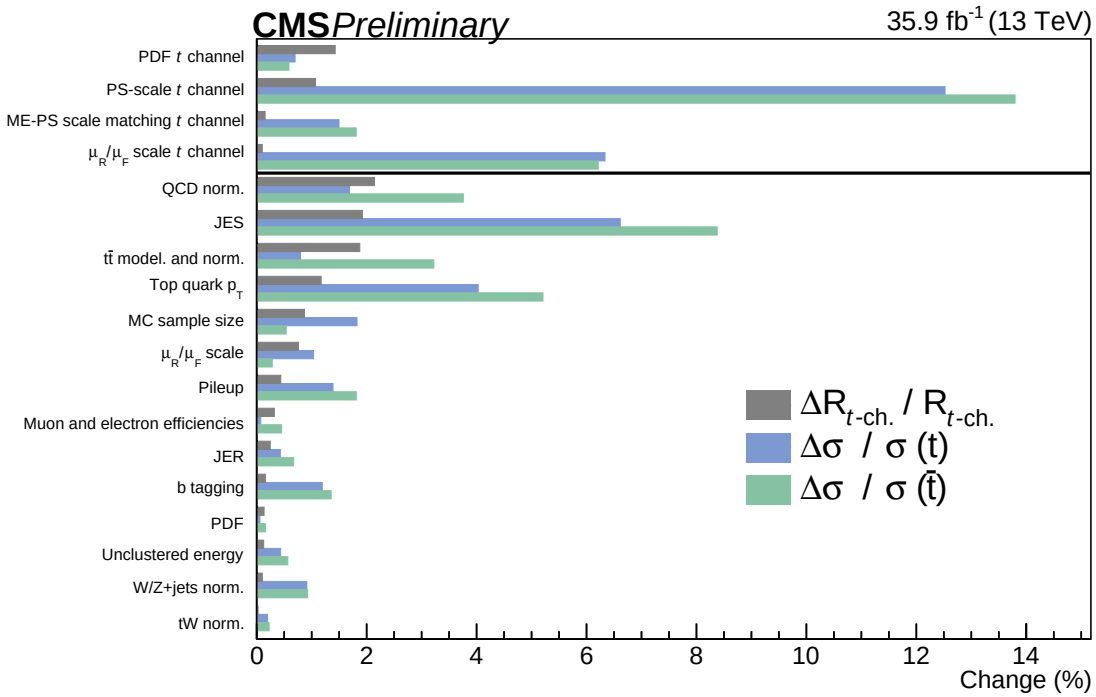

Figure 7: Estimated relative contributions of the listed uncertainty sources in % to the total uncertainties of the measured cross sections for top quark production and top antiquark production, and of the cross section ratio $R_{t\text{-ch.}}$. For the externalized signal modeling uncertainties, the values correspond to their relative uncertainties (first four entries). The other values are obtained by performing the fit again for each uncertainty source, with the corresponding nuisance parameter fixed to its optimal fit value and by calculating the resulting relative change in the cross sections, or cross section ratio, to the nominal ones.

Table 3: Estimated relative contributions of the listed uncertainty sources in % to the total uncertainties of the measured cross sections for top quark production and top antiquark production, and of the cross section ratio $R_{t\text{-ch.}}$. For the externalized signal modeling uncertainties, the values correspond to their relative uncertainties (first four entries). The other values are obtained by performing the fit again for each uncertainty source, with the corresponding nuisance parameter fixed to its optimal fit value and by calculating the resulting relative change in the cross sections, or cross section ratio, to the nominal ones.

	$\Delta R/R$	$\Delta\sigma/\sigma(\mathrm{t})$	$\Delta\sigma/\sigma(\bar{\mathrm{t}})$
PDF t channel	1.4	0.7	0.6
PS-scale t channel	1.1	12.5	13.8
ME-PS scale matching t channel	0.2	1.5	1.8
$\mu_\mathrm{R}/\mu_\mathrm{F}$ scale t channel	0.1	6.3	6.2
QCD normalization	2.1	1.7	3.8
JES	1.9	6.6	8.4
$\mathrm{t\bar{t}}$ modeling and normalization	1.9	0.8	3.2
Top quark p_T	1.2	4.0	5.2
MC sample size	0.9	1.8	0.5
$\mu_\mathrm{R}/\mu_\mathrm{F}$ scale	0.8	1.0	0.3
Pileup	0.4	1.4	1.8
Muon and electron efficiencies	0.3	0.1	0.5
JER	0.2	0.4	0.7
b tagging	0.2	1.2	1.4
PDF	0.1	0.1	0.2
Unclustered energy	0.1	0.4	0.6
W/Z+jets normalization	0.1	0.9	0.9
tW normalization	< 0.1	0.2	0.2

systematic uncertainty ("syst") is obtained by adding these two contributions in quadrature.

This ratio corresponds to the measured cross sections for the two processes of

$$\begin{aligned}\sigma_{t\text{-ch.,t}} &= 136.3 \pm 1.1\,(\text{stat}) \pm 3.4\,(\text{prof}) \pm 19.4\,(\text{ext}) \pm 3.4\,(\text{lumi})\,\text{pb}\\ &= 136.3 \pm 1.1\,(\text{stat}) \pm 20.0\,(\text{syst})\,\text{pb}\\ &= 136.3 \pm 20.0\,\text{pb},\\ \sigma_{t\text{-ch.,}\bar{\text{t}}} &= 82.7 \pm 1.1\,(\text{stat}) \pm 2.7\,(\text{prof}) \pm 12.6\,(\text{ext}) \pm 2.1\,(\text{lumi})\,\text{pb}\\ &= 82.7 \pm 1.1\,(\text{stat}) \pm 13.0\,(\text{syst})\,\text{pb}\\ &= 82.7 \pm 13.1\,\text{pb}.\end{aligned}$$

Here, the uncertainty due to the luminosity is labeled as "lumi". The total systematic uncertainty is obtained by adding the contributions from the luminosity uncertainty and from the profiled and externalized uncertainties in quadrature. The most dominant systematic uncertainty in the cross section measurements is the uncertainty in the parton shower scale of the t-channel signal process. The measurement of the cross section ratio is dominated by the uncertainties in the modeling of the $\mathrm{t\bar{t}}$ background contribution and by the PDF uncertainty of the signal process. The measured ratio is compared to the predictions of different PDF sets as shown in Fig. 8. Good agreement between the measurement and most predictions is found, except for the ABMP16 PDF set, which falls outside the uncertainty band of this measurement. Adding the $\sigma_{t\text{-ch.,t}}$ and $\sigma_{t\text{-ch.,}\bar{\text{t}}}$ results, the total cross section is found to be

$$\begin{aligned}\sigma_{t\text{-ch.,t}+\bar{\text{t}}} &= 219.0 \pm 1.5\,(\text{stat}) \pm 6.1\,(\text{prof}) \pm 32.0\,(\text{ext}) \pm 5.5\,(\text{lumi})\,\text{pb}\\ &= 219.0 \pm 1.5\,(\text{stat}) \pm 33.0\,(\text{syst})\,\text{pb}\\ &= 219.0 \pm 33.1\,\text{pb},\end{aligned}$$

where the statistical uncertainties are treated as uncorrelated and the systematic uncertainties as correlated between the $\sigma_{t\text{-ch.,t}}$ and $\sigma_{t\text{-ch.,}\bar{\text{t}}}$ measurements.

The total cross section is used to calculate the absolute value of the CKM matrix element $|V_{\text{tb}}|$ under the assumption that $|V_{\text{td}}|$ and $|V_{\text{ts}}|$ are significantly smaller than $|V_{\text{tb}}|$:

$$|\text{f}_{\text{LV}} V_{\text{tb}}| = \sqrt{\frac{\sigma_{t\text{-ch.,t}+\bar{\text{t}}}}{\sigma^{\text{theo}}_{t\text{-ch.,t}+\bar{\text{t}}}}},$$

with the predicted SM value $\sigma^{\text{theo}}_{t\text{-ch.,t}+\bar{\text{t}}} = 217.0^{+6.6}_{-4.6}\,(\text{scale}) \pm 6.2\,(\text{PDF}{+}\alpha_{\text{S}})\,\text{pb}$ [10, 11, 16] assuming $|V_{\text{tb}}| = 1$. The anomalous form factor f_{LV} takes the possible presence of an anomalous Wtb coupling into account, with $\text{f}_{\text{LV}} = 1$ for the SM and $\text{f}_{\text{LV}} \neq 1$ for physics beyond the standard model. The measured cross section translates to:

$$|\text{f}_{\text{LV}} V_{\text{tb}}| = 1.00 \pm 0.05\,(\text{exp}) \pm 0.02\,(\text{theo}).$$

The first uncertainty considers all uncertainties of the cross section measurement, while the second uncertainty is derived from the uncertainty of the theoretical SM prediction.

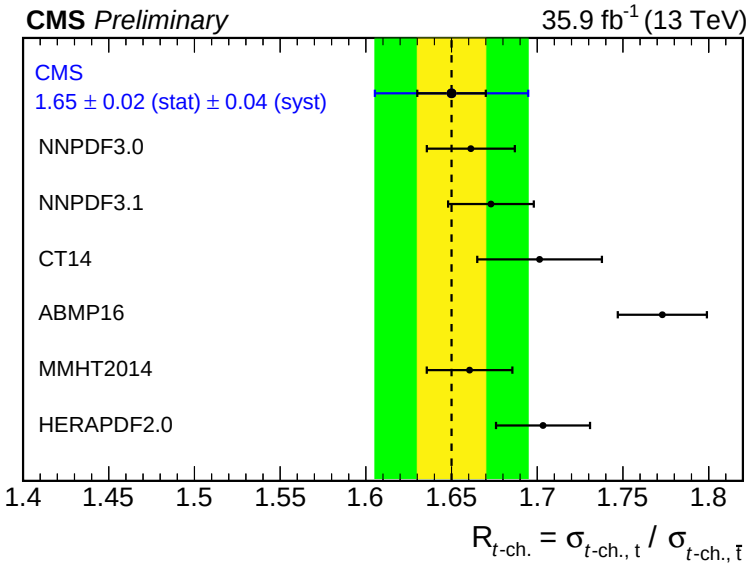

Figure 8: Comparison of the measured $R_{t\text{-ch.}}$ (dotted line) with the prediction from different PDF sets: NNPDF3.0 NLO[17], NNPDF3.1 NNLO [56], CT14 NLO [57], ABMP16 NNLO [58], MMHT2014 NLO [59], HERAPDF2.0 NLO [60]. The POWHEG 4FS calculation is used with a nominal value for the top quark mass of 172.5 GeV. The uncertainty bars for the different PDF sets include the statistical uncertainty, the uncertainty due to the factorization and renormalization scales, derived by varying both of them by a factor 0.5 and 2, and the uncertainty in the top quark mass, derived by varying the top quark mass between 171.5 and 173.5 GeV. For the measurement, the inner and outer uncertainty bars correspond to the statistical and total uncertainty, respectively.

8 Summary

A measurement of the ratio of the cross sections for the t-channel single top quark and single top antiquark production has been presented. The analysis uses events with one muon or electron and multiple jets in the final state to measure the cross sections for the production of single top quarks and of single top antiquarks, along with the ratio of the two processes. The measured ratio of the cross sections of the two processes of $R_{t\text{-ch.}} = 1.65 \pm 0.05$ is compared to recent predictions using different parton distribution functions (PDFs) to describe the inner structure of the proton. Good agreement with most PDF sets is found within the uncertainties of the measurement. The measured cross sections are $\sigma_{t\text{-ch.,t}} = 136.3 \pm 20.0\,\text{pb}$ for the production of single top quarks, $\sigma_{t\text{-ch.,}\bar{\text{t}}} = 82.7 \pm 13.1\,\text{pb}$ for the production of single top antiquarks, and $\sigma_{t\text{-ch.,t}+\bar{\text{t}}} = 219.0 \pm 33.1\,\text{pb}$ for the total cross section. The latter result is used to calculate the absolute value of the Cabibbo–Kobayashi–Maskawa matrix element $|f_{\text{LV}} V_{\text{tb}}| = 1.00 \pm 0.05\,(\text{exp}) \pm 0.02\,(\text{theo})$. All results are, within the reported uncertainties, in agreement with recent standard model predictions. With the increased data set used in this analysis, the statistical uncertainty plays only a minor role for the achieved precision of the measurement, which is limited by the systematic uncertainties in the modeling of the signal process. Deeper understanding of these effects and improved procedures to estimate the uncertainty are therefore crucial to further decrease the systematic uncertainty. Because of the cancellation of systematic effects when measuring the ratio of cross sections, the precision of the measurement of $R_{t\text{-ch.}}$ reported in this article is, however, significantly improved with respect to the results of previous measurements. The total uncertainty in the measured $R_{t\text{-ch.}}$ is now only about two times the size of the uncertainty in the predictions from theory and the

result can already be used to test the predictions from different PDF sets for their compatibility with measured data.

References

[1] N. Kidonakis, "Differential and total cross sections for top pair and single top production", *DESY-PROC* **2012-02/251** (2012) doi:10.3204/DESY-PROC-2012-02/251, arXiv:1205.3453.

[2] ATLAS Collaboration, "Measurement of the t-channel single top-quark production cross section in pp collisions at $\sqrt{s} = 7$ TeV with the ATLAS detector", *Phys. Lett. B* **717** (2012) 330, doi:10.1016/j.physletb.2012.09.031, arXiv:1205.3130.

[3] ATLAS Collaboration, "Comprehensive measurements of t-channel single top-quark production cross sections at $\sqrt{s} = 7$ TeV with the ATLAS detector", *Phys. Rev. D* **90** (2014) 112006, doi:10.1103/PhysRevD.90.112006, arXiv:1406.7844.

[4] ATLAS Collaboration, "Fiducial, total and differential cross-section measurements of t-channel single top-quark production in pp collisions at 8 TeV using data collected by the ATLAS detector", *Eur. Phys. J. C* **77** (2017) 531, doi:10.1140/epjc/s10052-017-5061-9, arXiv:1702.02859.

[5] ATLAS Collaboration, "Measurement of the inclusive cross-sections of single top-quark and top-antiquark t-channel production in pp collisions at $\sqrt{s}$ = 13 TeV with the ATLAS detector", *JHEP* **04** (2017) 086, doi:10.1007/JHEP04(2017)086, arXiv:1609.03920.

[6] CMS Collaboration, "Measurement of the t-channel single top quark production cross section in pp collisions at $\sqrt{s} = 7$ TeV", *Phys. Rev. Lett.* **107** (2011) 091802, doi:10.1103/PhysRevLett.107.091802, arXiv:1106.3052.

[7] CMS Collaboration, "Measurement of the single-top-quark t-channel cross section in pp collisions at $\sqrt{s} = 7$ TeV", *JHEP* **12** (2012) 035, doi:10.1007/JHEP12(2012)035, arXiv:1209.4533.

[8] CMS Collaboration, "Measurement of the t-channel single-top-quark production cross section and of the $| V_{tb} |$ CKM matrix element in pp collisions at $\sqrt{s}$= 8 TeV", *JHEP* **06** (2014) 090, doi:10.1007/JHEP06(2014)090, arXiv:1403.7366.

[9] CMS Collaboration, "Cross section measurement of t-channel single top quark production in pp collisions at $\sqrt{s} = 13$ TeV", *Phys. Lett. B* **772** (2017) 752, doi:10.1016/j.physletb.2017.07.047, arXiv:1610.00678.

[10] M. Aliev et al., "HATHOR: HAdronic Top and Heavy quarks crOss section calculatoR", *Comput. Phys. Commun.* **182** (2011) 1034, doi:10.1016/j.cpc.2010.12.040, arXiv:1007.1327.

[11] P. Kant et al., "HatHor for single top-quark production: Updated predictions and uncertainty estimates for single top-quark production in hadronic collisions", *Comput. Phys. Commun.* **191** (2015) 74, doi:10.1016/j.cpc.2015.02.001, arXiv:1406.4403.

[12] A. D. Martin, W. J. Stirling, R. S. Thorne, and G. Watt, "Parton distributions for the LHC", *Eur. Phys. J. C* **63** (2009) 189, doi:10.1140/epjc/s10052-009-1072-5, arXiv:0901.0002.

[13] A. D. Martin, W. J. Stirling, R. S. Thorne, and G. Watt, "Uncertainties on alpha(S) in global PDF analyses and implications for predicted hadronic cross sections", *Eur. Phys. J. C* **64** (2009) 653, doi:10.1140/epjc/s10052-009-1164-2, arXiv:0905.3531.

[14] H.-L. Lai et al., "New parton distributions for collider physics", *Phys. Rev. D* **82** (2010) 074024, doi:10.1103/PhysRevD.82.074024, arXiv:1007.2241.

[15] R. D. Ball et al., "Parton distributions with LHC data", *Nucl. Phys. B* **867** (2013) 244, doi:10.1016/j.nuclphysb.2012.10.003, arXiv:1207.1303.

[16] M. Botje et al., "The PDF4LHC Working Group Interim Recommendations", arXiv:1101.0538.

[17] R. D. Ball et al., "Parton distributions for the LHC Run II", *JHEP* **04** (2015) 040, doi:10.1007/JHEP04(2015)040, arXiv:1410.8849.

[18] CMS Collaboration, "The CMS experiment at the CERN LHC", *JINST* **3** (2008) S08004, doi:10.1088/1748-0221/3/08/S08004.

[19] P. Nason, "A New method for combining NLO QCD with shower Monte Carlo algorithms", *JHEP* **11** (2004) 040, doi:10.1088/1126-6708/2004/11/040, arXiv:hep-ph/0409146.

[20] S. Frixione, P. Nason, and C. Oleari, "Matching NLO QCD computations with Parton Shower simulations: the POWHEG method", *JHEP* **11** (2007) 070, doi:10.1088/1126-6708/2007/11/070, arXiv:0709.2092.

[21] S. Alioli, P. Nason, C. Oleari, and E. Re, "A general framework for implementing NLO calculations in shower Monte Carlo programs: the POWHEG BOX", *JHEP* **06** (2010) 043, doi:10.1007/JHEP06(2010)043, arXiv:1002.2581.

[22] S. Alioli, P. Nason, C. Oleari, and E. Re, "NLO single-top production matched with shower in POWHEG: s- and t-channel contributions", *JHEP* **09** (2009) 111, doi:10.1007/JHEP02(2010)011,10.1088/1126-6708/2009/09/111, arXiv:0907.4076. [Erratum: JHEP02,011(2010)].

[23] CMS Collaboration, "Measurements of the differential cross section of single top-quark production in the t channel in proton-proton collisions at $\sqrt{s}$ =8 TeV", Physics Analysis Summary CMS-PAS-TOP-14-004, CERN, 2014.

[24] S. Alioli, S.-O. Moch, and P. Uwer, "Hadronic top-quark pair-production with one jet and parton showering", *JHEP* **01** (2012) 137, doi:10.1007/JHEP01(2012)137, arXiv:1110.5251.

[25] E. Re, "Single-top Wt-channel production matched with parton showers using the POWHEG method", *Eur. Phys. J. C* **71** (2011) 1547, doi:10.1140/epjc/s10052-011-1547-z, arXiv:1009.2450.

[26] J. Alwall et al., "The automated computation of tree-level and next-to-leading order differential cross sections, and their matching to parton shower simulations", *JHEP* **07** (2014) 079, doi:10.1007/JHEP07(2014)079, arXiv:1405.0301.

[27] R. Frederix and S. Frixione, "Merging meets matching in MC@NLO", *JHEP* **12** (2012) 061, doi:10.1007/JHEP12(2012)061, arXiv:1209.6215.

[28] T. Sjöstrand et al., "An Introduction to PYTHIA 8.2", *Comput. Phys. Commun.* **191** (2015) 159, doi:10.1016/j.cpc.2015.01.024, arXiv:1410.3012.

[29] P. Skands, S. Carrazza, and J. Rojo, "Tuning PYTHIA 8.1: the Monash 2013 Tune", *Eur. Phys. J. C* **74** (2014) 3024, doi:10.1140/epjc/s10052-014-3024-y, arXiv:1404.5630.

[30] CMS Collaboration, "Investigations of the impact of the parton shower tuning in Pythia 8 in the modelling of $\mathrm{t\bar{t}}$ at $\sqrt{s} = 8$ and 13 TeV", CMS Physics Analysis Summary CMS-PAS-TOP-16-021, CERN, 2016.

[31] GEANT4 Collaboration, "GEANT4: A Simulation toolkit", *Nucl. Instrum. Meth. A* **506** (2003) 250–303, doi:10.1016/S0168-9002(03)01368-8.

[32] CMS Collaboration, "Particle-flow reconstruction and global event description with the CMS detector", *JINST* **12** (2017) P10003, doi:10.1088/1748-0221/12/10/P10003, arXiv:1706.04965.

[33] W. Adam, R. Frühwirth, A. Strandlie, and T. Todorov, "Reconstruction of electrons with the Gaussian-sum filter in the CMS tracker at the LHC", *J. Phys. G* **31** (2005) 9, doi:10.1088/0954-3899/31/9/N01, arXiv:physics/0306087.

[34] M. Cacciari, G. P. Salam, and G. Soyez, "The anti-k_t jet clustering algorithm", *JHEP* **04** (2008) 063, doi:10.1088/1126-6708/2008/04/063, arXiv:0802.1189.

[35] M. Cacciari, G. P. Salam, and G. Soyez, "FastJet User Manual", *Eur. Phys. J. C* **72** (2012) 1896, doi:10.1140/epjc/s10052-012-1896-2, arXiv:1111.6097.

[36] M. Cacciari and G. P. Salam, "Pileup subtraction using jet areas", *Phys. Lett. B* **659** (2008) 119, doi:10.1016/j.physletb.2007.09.077, arXiv:0707.1378.

[37] CMS Collaboration, "Jet energy scale and resolution in the CMS experiment in pp collisions at 8 TeV", *JINST* **12** (2017) P02014, doi:10.1088/1748-0221/12/02/P02014, arXiv:1607.03663.

[38] CMS Collaboration, "Identification of heavy-flavour jets with the CMS detector in pp collisions at 13 TeV", *JINST* **13** (2018) P05011, doi:10.1088/1748-0221/13/05/P05011, arXiv:1712.07158.

[39] CMS Collaboration, "Performance of missing energy reconstruction in 13 TeV pp collision data using the CMS detector", CMS Physics Analysis Summary CMS-PAS-JME-16-004, CERN, 2016.

[40] D0 Collaboration, "Observation of single top-quark production", *Phys. Rev. Lett.* **103** (2009) 092001, doi:10.1103/PhysRevLett.103.092001, arXiv:0903.0850.

[41] CDF Collaboration, "First observation of electroweak single top quark production", *Phys. Rev. Lett.* **103** (2009) 092002, doi:10.1103/PhysRevLett.103.092002, arXiv:0903.0885.

[42] A. Höcker et al., "TMVA - Toolkit for Multivariate Data Analysis", *PoS* **ACAT** (2007) 040, arXiv:physics/0703039.

[43] CMS Collaboration, "Determination of Jet Energy Calibration and Transverse Momentum Resolution in CMS", *JINST* **6** (2011) P11002, doi:10.1088/1748-0221/6/11/P11002, arXiv:1107.4277.

[44] CMS Collaboration, "Performance of the CMS missing transverse momentum reconstruction in pp data at $\sqrt{s}$ = 8 TeV", *JINST* **10** (2015) P02006, doi:10.1088/1748-0221/10/02/P02006, arXiv:1411.0511.

[45] CMS Collaboration, "Measurements of Inclusive W and Z Cross Sections in pp Collisions at $\sqrt{s} = 7$ TeV", *JHEP* **01** (2011) 080, doi:10.1007/JHEP01(2011)080, arXiv:1012.2466.

[46] CMS Collaboration, "Measurement of the inelastic proton-proton cross section at $\sqrt{s} =$ 13 TeV", *Submitted to: JHEP* (2018) arXiv:1802.02613.

[47] R. Barlow and C. Beeston, "Fitting using finite Monte Carlo samples", *Comp. Phys. Commun.* **77** (1993) 219, doi:https://doi.org/10.1016/0010-4655(93)90005-W.

[48] CMS Collaboration, "Measurement of the $t\bar{t}$ production cross section using events in the eμ final state in pp collisions at $\sqrt{s} = 13$ TeV", *Eur. Phys. J. C* **77** (2017) 172, doi:10.1140/epjc/s10052-017-4718-8, arXiv:1611.04040.

[49] CMS Collaboration, "Measurement of the differential cross section for top quark pair production in pp collisions at $\sqrt{s} = 8$ TeV", *Eur. Phys. J. C* **75** (2015) 542, doi:10.1140/epjc/s10052-015-3709-x, arXiv:1505.04480.

[50] CMS Collaboration, "Measurement of differential cross sections for top quark pair production using the lepton+jets final state in proton-proton collisions at 13 TeV", *Phys. Rev. D* **95** (2017) 092001, doi:10.1103/PhysRevD.95.092001, arXiv:1610.04191.

[51] CMS Collaboration, "Measurement of normalized differential $\mathrm{t\bar{t}}$ cross sections in the dilepton channel from pp collisions at $\sqrt{s} = 13$ TeV", *JHEP* **04** (2018) 060, doi:10.1007/JHEP04(2018)060, arXiv:1708.07638.

[52] CMS Collaboration, "Measurement of inclusive W and Z boson production cross sections in pp collisions at $\sqrt{s} = 13$ TeV", CMS Physics Analysis Summary CMS-PAS-SMP-15-004, CERN, 2015.

[53] CMS Collaboration, "Measurement of the production cross section for single top quarks in association with W bosons in proton-proton collisions at $\sqrt{s} = 13$ TeV", *Submitted to: JHEP* (2018) arXiv:1805.07399.

[54] A. Kalogeropoulos and J. Alwall, "The SysCalc code: A tool to derive theoretical systematic uncertainties", arXiv:1801.08401.

[55] CMS Collaboration, "CMS Luminosity Measurements for the 2016 Data Taking Period", CMS Physics Analysis Summary CMS-PAS-LUM-17-001, CERN, 2017.

[56] R. D. Ball et al., "Parton distributions from high-precision collider data", *Eur. Phys. J. C* **77** (2017) 663, doi:10.1140/epjc/s10052-017-5199-5, arXiv:1706.00428.

[57] S. Dulat et al., "New parton distribution functions from a global analysis of quantum chromodynamics", *Phys. Rev. D* **93** (2016) 033006, doi:10.1103/PhysRevD.93.033006, arXiv:1506.07443.

[58] S. Alekhin, J. Blümlein, S. Moch, and R. Placakyte, "Parton distribution functions, α_s, and heavy-quark masses for LHC Run II", *Phys. Rev. D* **96** (2017) 014011, doi:10.1103/PhysRevD.96.014011, arXiv:1701.05838.

[59] L. A. Harland-Lang, A. D. Martin, P. Motylinski, and R. S. Thorne, "Parton distributions in the LHC era: MMHT 2014 PDFs", *Eur. Phys. J. C* **75** (2015) 204, doi:10.1140/epjc/s10052-015-3397-6, arXiv:1412.3989.

[60] ZEUS, H1 Collaboration, "Combined Measurement and QCD Analysis of the Inclusive e+- p Scattering Cross Sections at HERA", *JHEP* **01** (2010) 109, doi:10.1007/JHEP01(2010)109, arXiv:0911.0884.